The Three-Link Nonholonomic Snake as a Hybrid Kinodynamic System

Tony Dear[1], Scott David Kelly[2], Matthew Travers[1], and Howie Choset[1]

***Abstract*— Motion planners often avoid the so-called singular configurations of a locomoting system because they can change a system's dynamics and cause it to incur unbounded input controller costs. However, such configurations can also allow a system to exhibit new modes of locomotion, which can be incorporated into previously established planning techniques. Here we take a nonholonomic kinematic system and present the formalism for representing it as a hybrid system taking advantage of the singular configuration and the associated dynamics. We show how to achieve the transition maps between the modes of operation by allowing actuated joints to become passive or locked, circumventing problems with unbounded constraint forces. This new model offers a new capability to take advantage of drift dynamics and rolling motions, which we demonstrate using a switching controller involving established kinematic techniques and preliminary dynamic maneuvers.**

I. INTRODUCTION

In mechanical systems, the notion of singularities has been extensively studied in the context of serial robotic manipulators [1]–[5]. For such systems, operating in a singular configuration usually entails the loss of a degree of freedom and consequently the loss of control. Mathematically, this is equivalent to a reduced rank in the mapping between joint and end-effector velocities. These systems thus usually avoid operating near such configurations or deploy controllers that actively stay away from them, although some take advantage of these properties for additional load-bearing capacity [6].

Singularities also appear in locomoting systems, most notably legged robots and snake-like robots, as both consist of kinematic chain structures and can potentially suffer the same problems as manipulators. Much analysis has been produced for legged robot singularities in the guise of parallel manipulators [7], [8], but practically these systems cannot stretch out their legs, with few exceptions [9]. Similarly, many controllers have been proposed that actively avoid the straight or arc configurations in snake robots [10], [11].

Other types of locomoting systems can exhibit singularities as well, such as the nonholonomic Snakeboard [12]. Like the aforementioned examples, these configurations can lead to a loss of degree of freedom or a completely different set of dynamics, features generally undesirable for locomotion. However, it has been shown that by separately coming up with an appropriate model or controller for these configurations, they can still be interesting and useful. In particular, the turn-in-place configuration was observed by Ostrowski et al. [13] and later incorporated, along with the straight-line configuration, into a motion planner by Dear et al. [14].

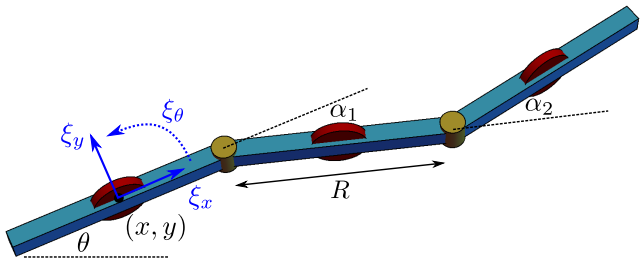

Fig. 1: A three-link nonholonomic robot. The coordinates (x, y, θ) describe the inertial position and orientation of the first link, which can also be described in a body-attached frame with velocities $(\xi_x, \xi_y, \xi_\theta)$. The joint angles (α_1, α_2) describe the relative configurations of the links thereafter.

Because of the potential discontinuities in the evolution of a system's state when going into a singular configuration, it is natural to represent these systems in a hybrid manner, in which we actually have two or more subsystems with different dynamics. The transitions between the different subsystems must also be defined appropriately. An initial approach was shown on manipulators by Tan et al. [15], who devised a switching hybrid controller that accommodated the robot near or even at the singularities.

In this paper, we formally introduce this representation for the three-link nonholonomic snake robot, shown in Fig. 1. In previous literature, this system was also known as the three-link *kinematic* snake [16]–[18], so named because its three constraints eliminate the need to consider second-order dynamics (accelerations) in normal operation. However, this classification is insufficient when considering the arc singular configuration, shown in Fig. 2, as the constraints no longer fully prevent the system from moving dynamically due to built-up momentum. We thus call this a *hybrid kinodynamic system*.

The rest of this paper is organized as follows. Section II introduces the standard reduced kinematic model of the nonholonomic snake system, and we show how to extend this to a hybrid framework when considering the dynamics of the singular arc configuration. Although we show in Section III that there are problems with the physical feasibility of using this model, the same ideas will be used to derive an alternate model involving a hybrid active-passive switching controller in an environment with external forcing. After presenting an example motion planning trajectory utilizing these ideas, we conclude with future directions in Section IV.

[1]T. Dear, M. Travers, and H. Choset are with the Robotics Institute at Carnegie Mellon University, Pittsburgh, PA 15213, USA. {tonydear@, mtravers@andrew., choset@cs.}cmu.edu

[2]S. D. Kelly is with the Department of Mechanical Engineering and Engineering Science at the University of North Carolina at Charlotte, Charlotte, NC 28223, USA. scott@kellyfish.net

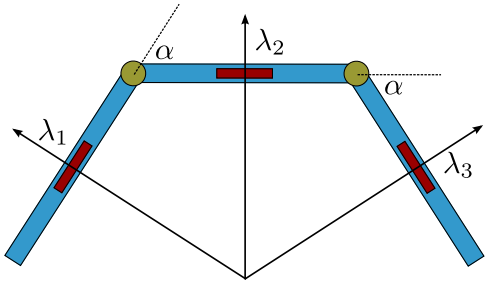

Fig. 2: The robot in an arc singular configuration, where $\alpha_1 = \alpha_2 = \alpha$. Notice that the directions of the three constraint forces $(\lambda_1, \lambda_2, \lambda_3)$ all intersect at a common point, meaning that one is redundant given the other two.

II. MECHANICAL MODEL OF THE SNAKE

We present the reduced mathematical formulation of the robot's locomotion. Away from singularities, the system's nonholonomic constraints make it a kinematic system, a model that has been studied rigorously in the literature. We then introduce the dynamic model in the singular configuration, allowing us to represent the system as a hybrid system when combined with the kinematic model.

A. Kinematic Model (Normal Operation)

As shown in Fig. 1, the robot consists of three rigid links, each of length R, which can rotate relative to one another. Its configuration can be written as $q \in Q = G \times M$, where $g = (x, y, \theta)^T \in G = SE(2)$ specifies the position and orientation of the first link in an inertial frame; we measure a link's position at the center of the link. The joint angles $r = (\alpha_1, \alpha_2)^T \in M$ specify the links' relative orientation as shown. We can view Q as a principal fiber bundle, in which trajectories in the shape or base space M lift to trajectories in the group G [19]. We thus take r to be the actuated inputs of the system; we do not assume joint limits in this paper.

The wheels at the centers of the links provide a set of nonholonomic constraints that restrict the system's motion. Each of the constraints can be written in the form

$$-\dot{x}_i \sin\theta_i + \dot{y}_i \cos\theta_i = 0, \tag{1}$$

where $(\dot{x}_i, \dot{y}_i)$ is the velocity and θ_i is the orientation of the ith link. These quantities can be found via the system's geometry and written in terms of the configuration coordinates and velocities. The group and shape velocity components can be separated in Pfaffian form [18] as

$$\omega_g(q)\dot{g} + \omega_r(r)\dot{r} = 0, \tag{2}$$

where $\omega_g \in \mathbb{R}^{3\times 3}$ and $\omega_r \in \mathbb{R}^{3\times 2}$.

Since the number of independent constraints is equal to the dimension of the group, these equations are sufficient to derive a kinematic connection for the system [18]. In other words, the constraint equations fully describe the first-order dynamics of the group variables in terms of the shape variables only. They can be rearranged to show this explicitly as the *kinematic reconstruction equation*:

$$\xi = -\underbrace{\frac{1}{D}\begin{pmatrix} \frac{R}{2}(\cos\alpha_1 + \cos(\alpha_1 - \alpha_2)) & \frac{R}{2}(1 + \cos\alpha_1) \\ 0 & 0 \\ \sin\alpha_1 + \sin(\alpha_1 - \alpha_2) & \sin\alpha_1 \end{pmatrix}}_{\mathbf{A}(r)} \dot{r}, \tag{3}$$

where $D = \sin\alpha_1 + \sin(\alpha_1 - \alpha_2) - \sin\alpha_2$. The matrix $\mathbf{A}(r)$ is called the principal kinematic connection, a mapping that depends only on the shape variables, in this case α_1 and α_2. The variables $\xi = (\xi_x, \xi_y, \xi_\theta)^T$ give us the velocity of the system written in a body-attached frame, as shown in Fig. 1. In $SE(2)$, the mapping that takes body velocities to inertial velocities is given by $\dot{g} = T_e L_g \xi$, where

$$T_e L_g = \begin{pmatrix} \cos\theta & -\sin\theta & 0 \\ \sin\theta & \cos\theta & 0 \\ 0 & 0 & 1 \end{pmatrix}. \tag{4}$$

In the literature, the kinematic model (3) has yielded rich insights into the system's locomotion. Ostrowski and Burdick [16] developed gaits, or periodic inputs for $\dot{r}$, that allowed the robot to undulate and rotate in place. Shammas et al. [18] and Hatton and Choset [20] studied the structure of the connection in the form of height functions and vector fields in order to achieve motion in specific directions.

B. Dynamic Model in Singular Configurations

It can be observed that when the robot is in a configuration with $\alpha = \alpha_1 = \alpha_2$, the kinematic model is no longer valid; in Eq. (3), the denominator D goes to 0 when this occurs. This is because the constraints themselves become redundant, causing the matrix ω_g in Eq. (2) to lose rank. Geometrically, the constraint directions intersect at a common point, as shown in Fig. 2, because any one of the constraints is redundant given the other two.

Since the constraints are no longer sufficient to fully describe the system's locomotion, we require the second-order dynamics to supplement these equations. Assigning each of the links identical masses m and inertias J, the system's Lagrangian is given by its kinetic energy

$$L(q, \dot{q}) = T(q, \dot{q}) = \sum_{i=1}^{3} \left(\frac{1}{2} m(\dot{x}_i^2 + \dot{y}_i^2) + \frac{1}{2} J \dot{\theta}_i^2 \right). \tag{5}$$

Since the joint angles are now equal, we only need to track one shape variable, which we will denote as α. Substitution of $\alpha_1 = \alpha_2$ into the constraints (2) yields a restriction on the velocities such that $\dot{\alpha}_1 = -\dot{\alpha}_2$. Since we assume that the constraints are ideal, we will enforce this condition in the following computations as well.

Following the formalism of Bloch et al. [21], we are now in a position to compute the momentum for the system by considering the allowable directions of motion. Since any velocity that satisfies two of the constraints will satisfy the third, we can take any two of the three rows of ω_g from Eq. (2), make the aforementioned substitutions, and obtain the reduced constraints

$$\tilde{\omega}_g(q)\dot{g} + \tilde{\omega}_\alpha(\alpha)\dot{\alpha} = 0 \tag{6}$$

with $\tilde{\omega}_g \in \mathbb{R}^{2\times 3}$ and $\tilde{\omega}_\alpha \in \mathbb{R}^{2\times 1}$. Allowed group velocities live in the null space of $\tilde{\omega}_g$, which is given by

$$\tilde{D}_q = \text{span}(R\cos\theta, R\sin\theta, 2\tan(\alpha/2))^T. \tag{7}$$

We take the generalized momentum derived from the Lagrangian (5) as $\frac{\partial L}{\partial \dot{g}}$ and project it onto $\tilde{D}_q$. This gives us an expression for the *generalized nonholonomic momentum* p, which can be written as a linear combination of group and shape velocity components as

$$p = \eta_g(q)\dot{g} + \eta_\alpha(\alpha)\dot{\alpha}, \tag{8}$$

where $\eta_g \in \mathbb{R}^{1\times 3}$ and η_α is a scalar function of α only. Stacking Eqs. (6) and (8) together gives us three independent equations, which can be rearranged in the same way as the original constraints to produce a new reconstruction equation, which takes the form

$$\xi = -A(\alpha)\dot{\alpha} + \Gamma(\alpha)p. \tag{9}$$

$A(\alpha)$ is called the local form of the mechanical connection, while $\Gamma(\alpha)$ is the local form of the locked inertia tensor [17], [18]. The system's locomotion is thus determined by a combination of actuation in α and momentum in p.

Practically, we know that these dynamics only apply when the system is in a configuration in which the joint angles are equal. If $\dot{\alpha} \neq 0$, the two joint angles will instantaneously move in opposite directions, violating the initial assumption and behaving kinematically once again. We can thus use a simplified model where only $\dot{\alpha} = 0$ is allowed:

$$\xi = \Gamma(\alpha)p = \frac{(R(1+\cos\alpha), 0, 2\sin\alpha)^T p}{3(mR^2 + 4J + (mR^2 - 4J)\cos\alpha)}. \tag{10}$$

In addition, p is conserved ($\dot{p} = 0$) since there are no dissipative forces acting on the system and the system moves as a single rigid body. Eq. (10) thus shows that the robot is only able to move dynamically if starting with some nonzero initial momentum p_0 in this regime.

C. Full Hybrid Kinodynamic Model

Now that we have the respective system behaviors under each mode of operation, we can put them together into a complete hybrid model. We consider splitting the configuration tangent bundle as $TQ \supset TQ_k \times TQ_d$, where

$$TQ_k = \{(q,\dot{q}) \in TQ \mid \alpha_1 \neq \alpha_2\},$$
$$TQ_d = \{(q,\dot{q}) \in TQ \mid \alpha_1 = \alpha_2,\ \dot{\alpha}_1 = -\dot{\alpha}_2\}.$$

TQ is a proper superset of $TQ_k \times TQ_d$, since the states in which $\alpha_1 = \alpha_2$, $\dot{\alpha}_1 \neq -\dot{\alpha}_2$ do not belong in either subset.

We also define the *guards*, or regions of the tangent bundle in which transitions occur. These will be written as

$$S_k = \{(q,\dot{q}) \in TQ_k \mid |\alpha_1 - \alpha_2| < \delta,\ \dot{\alpha}_1 = -\dot{\alpha}_2\},$$
$$S_d = \{(q,\dot{q}) \in TQ_d \mid |\dot{\alpha}_1| \neq 0\}.$$

Here $\delta > 0$ is a small number that dictates at which point the dynamic model should replace the kinematic one. In this work, we consider the switching timescale to be small enough that a discrete transition model is sufficient; a continuous kinematic-dynamic transition may be the subject of future work. The velocity requirement on S_k ensures that we switch only when it is meaningful; if the joint velocities are not equal and opposite, then the original constraints would be violated when we are sufficiently close to the singular configuration.

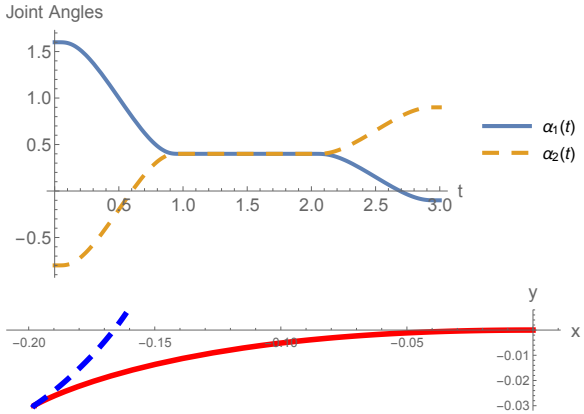

Fig. 3: Simulation starting at different joint angles and converging with equal and opposite velocities to the same value at $t = 1$. The robot is in the singular configuration for a finite period of time before going back to kinematic operation at $t = 2$, again with equal and opposite velocities. The resultant trajectory for each of the kinematic modes is shown below in red solid and blue dashed, respectively.

Finally, we define the *transition maps*, which describe how configurations map from one model to the other. The first map $\Delta_k : S_k \to TQ_d$ assigns the joint angles to their original limit value, while making the joint velocities 0. The nonholonomic momentum p is defined according to Eq. (8), while the group configuration remains unchanged. Going in the other direction, the map $\Delta_d : S_d \to TQ_k$ leaves the joint velocities and group configuration unchanged, but p becomes instantaneously 0 and the group velocities are reassigned according to the kinematic model. The joint angles must differ by a small number ϵ in order to evaluate the kinematic model, becoming $(\alpha+\epsilon, \alpha-\epsilon)$. Both transition maps can thus cause the state of the system to experience discrete jumps.

Putting everything together, our hybrid model can be written as follows.

$$\begin{cases} \xi = -\mathbf{A}(r)\dot{r}, & (q,\dot{q}) \in TQ_k \backslash S_k \\ (q,\dot{q})^+ = \Delta_k((q,\dot{q})^-), & (q,\dot{q})^- \in S_k \\ \xi = -A(\alpha)\dot{\alpha} + \Gamma(\alpha)p, & (q,\dot{q}) \in TQ_d \backslash S_d \\ (q,\dot{q})^+ = \Delta_d((q,\dot{q})^-), & (q,\dot{q})^- \in S_d \end{cases} \tag{11}$$

The models in each case are described respectively by Eqs. (3) and (9). For the transition cases, the superscripts $-$ and $+$ refer to the system's state before and after the transition, respectively.

III. MOTION PLANNING APPLICATION

Without regard to the torques of the joint inputs, Eq. (11) sufficiently describes the evolution of the system assuming

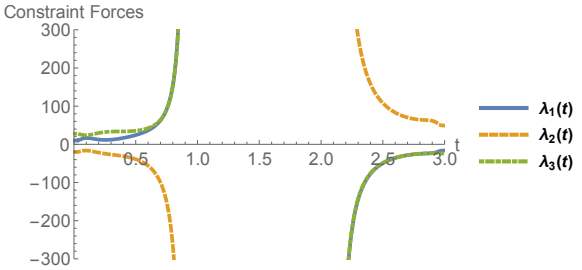

Fig. 4: The constraint forces become unbounded when the joint angles become close to equal, even though the velocity condition satisfies the constraints. This phenomenon is not captured by the reduced model.

we can command the joint velocities directly. As shown in Fig. 3, we can start the joints at different angles and move them such that they smoothly approach the same value in finite time with equal and opposite velocities, and the system is considered to be in the dynamic mode at $t = 1$, albeit with zero momentum. Then we jump back into the kinematic mode by actuating the joints again, starting with opposite values of velocity at $t = 2$ and proceeding kinematically afterward, at which point there is no longer a restriction on the joint velocities. In this and all simulations that follow, we set the parameters m, J, and R to 1.

Aside from the fact that it is seemingly not possible to make the transition into the dynamic mode with nonzero momentum (since joint velocities must go to 0 in order for the system remain in it), a practical issue arises when considering the second-order torques required for this model. To see this, we consider the constraint forces acting on the wheels for the types of trajectories allowed above. If we use the Euler-Lagrange formulation, these forces are given by the Lagrange multipliers $\lambda = (\lambda_1, \lambda_2, \lambda_3)^T$. In addition to the constraint equations, the full equations of motion include

$$\frac{d}{dt}\left(\frac{\partial L(q,\dot{q})}{\partial \dot{q}^i}\right) - \frac{\partial L(q,\dot{q})}{\partial q^i} = (\omega_g)_i \lambda. \tag{12}$$

We will neglect the dynamics of the joints themselves (we assume that they can be fully integrated and are thus known), so we have one equation for each of the three group variables. The object $(\omega_g)_i$ refers to the ith row of ω_g in Eq. (2).

If we take the joint inputs and output trajectory shown in Fig. 3 and plug them into the Euler-Lagrange equations, we can solve a system of equations for the three λ variables as functions of time. As shown in Fig. 4, all three become unbounded as the system approaches the singular configuration. This behavior was not apparent at the joint level when considering velocities alone as the constraints remained satisfied throughout the transition from kinematic to the dynamic model.

A. External Forcing and Passive Joints

It is clear that the three-link robot is unable to move into the singular configuration if the constraints are non-ideal; in a physical system, the large constraint forces would cause the wheels to slip after a certain point. Moreover, even assuming that the wheels can withstand infinite forces, the dynamics are not very interesting since the system cannot make the transition with nonzero velocity. Hence, we propose study of this robot in the presence of external forcing, for example in the form of gravity by placing the robot on an incline, and derive a new control strategy for achieving these transitions in a non-trivial manner.

Gravity introduces a potential energy term in the form of

$$U_\beta = m\beta \sum_{i=1}^{3} y_i, \tag{13}$$

which can be subtracted from the kinetic energy (5) to form a new Lagrangian $L_\beta = T - U_\beta$. Here β governs the strength of the gravitational force. A second modification to our system will allow for a joint to switch to being passive, so that its motion is determined solely by the Lagrangian equations of motion. The study of passive joint dynamics in underactuated manipulators has received some attention in the literature [22], [23], including analysis of controllability and coupling dynamics. Li et al. [24] studied a mobile manipulator with a hybrid switching joint, similar to what we propose here.

When a joint becomes passive, the three-link robot is governed by second-order dynamics even if $\alpha_1 \neq \alpha_2$. While all three constraints remain in play, we gain an unactuated degree of freedom in the passive joint. The idea is thus to allow gravity to "pull" the system into the singular configuration since internal actuation alone is insufficient to do so. On the other hand, the introduction of gravity does not affect the robot's kinematic operation when both joints are actuated, as the three constraints sufficiently determine the evolution of the three group variables.

The presence of gravity means that the group symmetries are broken—specifically, the Lagrangian L_β now has an explicit dependence on the group configuration. This prevents us from deriving a set of reduced equations for the system in the form of Eq. (9); instead, we revert to using the full Euler-Lagrange equations when a joint becomes passive. The three equations corresponding to the group variables can be rederived using L_β according to Eq. (12), and we include a fourth equation for the passive joint:

$$\frac{d}{dt}\left(\frac{\partial L_\beta(q,\dot{q})}{\partial \dot{\alpha}^j}\right) - \frac{\partial L_\beta(q,\dot{q})}{\partial \alpha^j} = (\omega_r)_j \lambda. \tag{14}$$

The λ is again the vector of constraint forces, while $(\omega_r)_j$ is the row of $\omega_r(r)$ from Eq. (2) corresponding to the unactuated joint.

In order to relate this new dynamic model to the fully acutuated kinematic one, which is still governed by the reduced equations (3), we can view both as part of a larger hybrid representation of a kinodynamic system. The guards are determined by the controller chosen, as we assume that we can fully control when the hybrid joint switches between the two modes. The kinematic-to-dynamic transition map Δ_k is trivially the identity mapping; all the unactuated degrees of freedom take their current values as the initial conditions

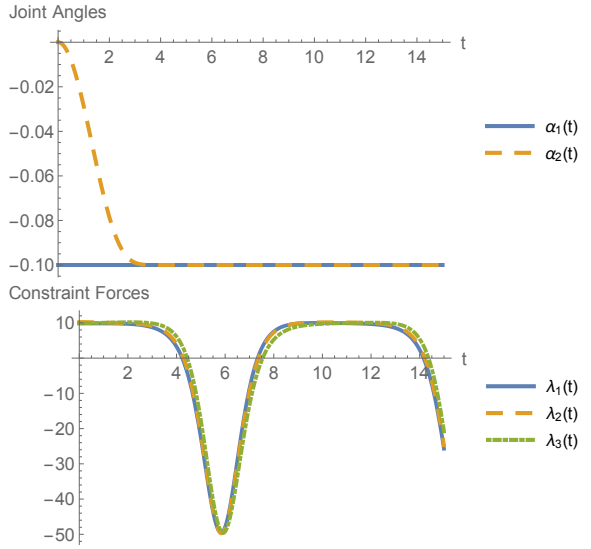

Fig. 5: Simulation showing the passive joint α_2 converging to the value of the locked joint α_1 while constraint forces remain bounded. The constraint forces are periodic due to the now arc-shaped system oscillating on the hill.

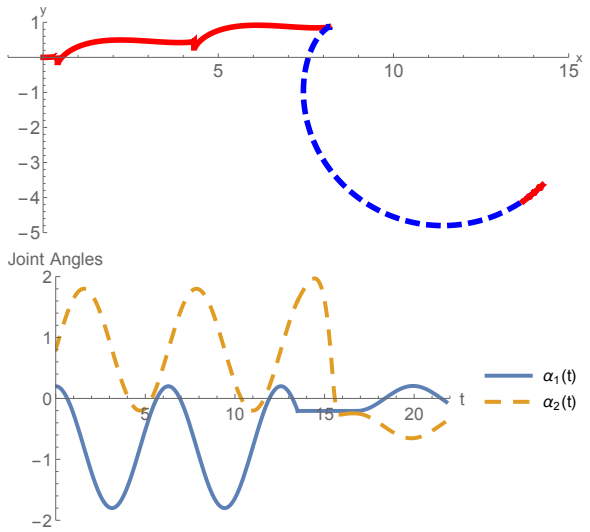

Fig. 6: Illustration of a switching controller on the full hybrid model in a gravitational force field. Red portions of the trajectory indicate kinematic control, while the blue (dashed) portion indicates a locked-passive joint configuration acted upon by external forcing.

for evolution according to the Lagrange equations. We define the reverse transition map Δ_d similarly and map the same configuration and velocity values back over to the kinematic model. This will ensure that the system moves continuously, since the kinematic equations (3) are always satisfied under the dynamic equations as the system moves.

B. Switching Controller

In order to show that our new arrangement solves the earlier problem of unbounded constraint forces, consider the simulation results shown in Fig. 5, with β set to 10. Here we start the system with $\theta = 0.1$ and $\alpha = (-0.1, 0)^T$, so that the first link is oriented "downward" while the other two are horizontal with respect to the slope direction. By keeping α_1 locked and leaving α_2 passive, the system obeys the dynamic equations and starts moving down the hill. At the same time, we see that the passive joint converges to the value of the locked one, naturally moving into a singular configuration. This occurs with the constraint forces remaining finite, as opposed to the behavior observed in Fig. 4.

A simple observation about the stability of such a maneuver and the singular configuration can be made using a standard Lyapunov function $V(\alpha) = (\alpha_1 - \alpha_2)^2$. It is positive as long as $\alpha_1 \neq \alpha_2$. We can then compute the time derivative

$$\dot{V}(\alpha) = 2(\alpha_1 - \alpha_2)(\dot{\alpha}_1 - \dot{\alpha}_2). \tag{15}$$

For the simulation above, $\dot{\alpha}_1 = 0$ and α_2 starts at a greater value than α_1. Since gravity pulls on the system such that $\dot{\alpha}_2$ is negative from the starting configuration, we have that $\dot{V}$ is negative and the singular configuration is asymptotically stable in this particular domain.

In general, Eq. (15) says that the singular configuration is stable as long as gravity is either opening or closing the passive joint to match the locked one. For example, we would not have the same guarantee if we kept the same initial conditions as the previous simulation but flipped the robot around so that $\theta = \pi + 0.1$. Gravity would pull in the opposite direction and tend to "open" α_2 away from α_1. Another consideration is that such a statement only holds starting from rest; after the system gets moving, its momentum may interact with gravity to produce non-trivial joint behavior.

These observations suggest a switching controller for maneuvering downward on a hill without joint actuation. By starting at rest and locking one joint, the system will converge to the singular configuration and traverse an arc down the hill with a curvature determined by the locked joint angle. To stop anywhere along the resultant trajectory, both joints can be actuated from zero with opposite velocities, popping the system out of the singular configuration and leaving us with full kinematic control once again.

Fig. 6 shows an example of such a composite trajectory combining a kinematic controller with dynamic movement. Shammas et al. [18] details the system's height functions, given by the rows of the kinematic connection (3), which can be used to find gaits for the two joints that achieve motion in a specific direction. For the first part of our trajectory, we use the simple gaits

$$\alpha_1(t) = \cos t - 0.8,$$
$$\alpha_2(t) = \sin t + 0.8,$$

which avoid singularities and locomote the system mostly in the x direction with some displacement in y. The first red solid portion of the trajectory plot shows the resultant movement from time $t = 0$ to $t = 13.5$.

The second part of the trajectory, shown in blue dashed, involves the system rolling dynamically down the hill starting

from its current group configuration. We lock α_1 at its value at $t = 13.5$; practically, any other desired value can also be chosen since we still assume full control of the joint, and the locked angle determines the curvature of the trajectory undertaken by the system. For α_2, we make it passive starting from its current value, but it can also be reoriented closer to α_1 if necessary. As shown in the joint angles plot, α_2 moves toward α_1, overshoots, and corrects back as the system rolls down along the circle trajectory. With the joint angles staying so close together, such a maneuver would incur high constraint forces if relying on internal joint actuation.

In the third and final segment, we again assume full kinematic control of the system. From the current values of the joint angles at $t = 16.8$ we start actuating both joints with opposite velocities to move them away from each other. The last segment traveled is shown in the rightmost part of the trajectory in red in Fig. 6. The joint angles may now be controlled, again with the aid of height functions or other kinematic tools, to approach the most appropriate gaits for the next part of the desired trajectory.

IV. CONCLUSIONS AND FUTURE WORK

To the authors' knowledge, this is the first application of hybrid systems analysis to locomoting systems with group symmetries and the corresponding reduced equations. In addition to showing how the three-link robot in particular straddles the boundary between kinematic and dynamic systems, we presented a model able to incorporate singular configurations. Although we considered a situation in which the group symmetries were broken in dynamic operation, the hybrid framework was still useful for accommodating hybrid joints and switching controllers, ideas also little explored so far in this literature.

Because of the variety of ideas explored in this paper, a number of opportunities exist for future work. It is conceivable that manipulator research on hybrid systems with singularities [15], [24] and passive joint behaviors [22], [23] can be carried over to or inspire locomotion research in the same areas. Specifically for the three-link snake, the work in this paper may benefit from a more thorough description of the singular configuration stability for motion planning, including what happens when the locked joint is actuated instead of simply locked. A natural extension of this system would be analysis of the general n-link snake robot, with $n > 3$. Finally, the big picture would be to establish this formalism for a general class of locomoting systems that can demonstrate hybrid dynamics or behavior, such as the Snakeboard [14].

REFERENCES

[1] S.-L. Wang and K. J. Waldron, "A study of the singular configurations of serial manipulators," *Journal of Mechanical Design*, vol. 109, no. 1, pp. 14–20, 1987.

[2] J.-P. Merlet, "Singular configurations of parallel manipulators and grassmann geometry," *The International Journal of Robotics Research*, vol. 8, no. 5, pp. 45–56, 1989.

[3] C. Gosselin and J. Angeles, "Singularity analysis of closed-loop kinematic chains," *Robotics and Automation, IEEE Transactions on*, vol. 6, no. 3, pp. 281–290, Jun 1990.

[4] D. Zlatanov, R. Fenton, and B. Benhabib, "A unifying framework for classification and interpretation of mechanism singularities," *Journal of Mechanical Design*, vol. 117, no. 4, pp. 566–572, 1995.

[5] P. Donelan, "Singularities of robot manipulators," *Singularity Theory*, pp. 189–217, 2007.

[6] J. Kieffer and J. Lenarcic, "On the exploitation of mechanical advantage near robot singularities," *Informatica*, vol. 18, no. 3, pp. 315–323, 1994.

[7] G. Yang, I.-M. Chen, W. Lin, and J. Angeles, "Singularity analysis of three-legged parallel robots based on passive-joint velocities," *Robotics and Automation, IEEE Transactions on*, vol. 17, no. 4, pp. 413–422, Aug 2001.

[8] P. Ben-Horin and M. Shoham, "Singularity condition of six-degree-of-freedom three-legged parallel robots based on grassmann-cayley algebra," *Robotics, IEEE Transactions on*, vol. 22, no. 4, pp. 577–590, Aug 2006.

[9] Y. Ogura, K. Shimomura, H. Kondo, A. Morishima, T. Okubo, S. Momoki, H. ok Lim, and A. Takanishi, "Human-like walking with knee stretched, heel-contact and toe-off motion by a humanoid robot," in *Intelligent Robots and Systems, 2006 IEEE/RSJ International Conference on*, Oct 2006, pp. 3976–3981.

[10] C. Ye, S. Ma, B. Li, and Y. Wang, "Locomotion control of a novel snake-like robot," in *Intelligent Robots and Systems, 2004. (IROS 2004). Proceedings. 2004 IEEE/RSJ International Conference on*, vol. 1, Sept 2004, pp. 925–930 vol.1.

[11] F. Matsuno and H. Sato, "Trajectory tracking control of snake robots based on dynamic model," in *Robotics and Automation, 2005. ICRA 2005. Proceedings of the 2005 IEEE International Conference on*, April 2005, pp. 3029–3034.

[12] J. Ostrowski, A. Lewis, R. Murray, and J. Burdick, "Nonholonomic mechanics and locomotion: the snakeboard example," in *Robotics and Automation, 1994. Proceedings., 1994 IEEE International Conference on*, May 1994, pp. 2391–2397 vol.3.

[13] J. P. Ostrowski, J. P. Desai, and V. Kumar, "Optimal gait selection for nonholonomic locomotion systems," *The International Journal of Robotics Research*, vol. 19, no. 3, pp. 225–237, 2000.

[14] T. Dear, R. L. Hatton, M. Travers, and H. Choset, "Snakeboard motion planning with local trajectory information," in *ASME 2013 Dynamic Systems and Control Conference*. American Society of Mechanical Engineers, 2013, pp. V002T33A002–V002T33A002.

[15] J. Tan, N. Xi, and Y. Wang, "A singularity-free motion control algorithm for robot manipulatorsa hybrid system approach," *Automatica*, vol. 40, no. 7, pp. 1239 – 1245, 2004.

[16] J. Ostrowski and J. Burdick, "Gait kinematics for a serpentine robot," in *Robotics and Automation, 1996. Proceedings., 1996 IEEE International Conference on*, vol. 2, Apr 1996, pp. 1294–1299 vol.2.

[17] J. Ostrowski, "Computing reduced equations for robotic systems with constraints and symmetries," *Robotics and Automation, IEEE Transactions on*, vol. 15, no. 1, pp. 111–123, Feb 1999.

[18] E. A. Shammas, H. Choset, and A. A. Rizzi, "Geometric motion planning analysis for two classes of underactuated mechanical systems," *The International Journal of Robotics Research*, vol. 26, no. 10, pp. 1043–1073, 2007.

[19] S. D. Kelly and R. M. Murray, "Geometric phases and robotic locomotion," *Journal of Robotic Systems*, vol. 12, no. 6, pp. 417–431, 1995.

[20] R. L. Hatton and H. Choset, "Geometric motion planning: The local connection, stokes theorem, and the importance of coordinate choice," *The International Journal of Robotics Research*, vol. 30, no. 8, pp. 988–1014, 2011.

[21] A. Bloch, P. Krishnaprasad, J. Marsden, and R. Murray, "Nonholonomic mechanical systems with symmetry," *Archive for Rational Mechanics and Analysis*, vol. 136, no. 1, pp. 21–99, 1996.

[22] M. Bergerman, C. Lee, and Y. Xu, "A dynamic coupling index for underactuated manipulators," *Journal of Robotic Systems*, vol. 12, no. 10, pp. 693–707, 1995.

[23] H. Arai, K. Tanie, and N. Shiroma, "Nonholonomic control of a three-dof planar underactuated manipulator," *Robotics and Automation, IEEE Transactions on*, vol. 14, no. 5, pp. 681–695, Oct 1998.

[24] Z. Li, A. Ming, N. Xi, and M. Shimojo, "Motion control of nonholonomic mobile underactuated manipulator," in *Robotics and Automation, 2006. ICRA 2006. Proceedings 2006 IEEE International Conference on*, May 2006, pp. 3512–3519.